Published in final edited form as:
Mol Microbiol. 2014 August ; 93(3): 568–581. doi:10.1111/mmi.12680.

Functional Mapping of Community Acquired Respiratory Distress Syndrome (CARDS) Toxin of *Mycoplasma pneumoniae* Defines Regions with ADP-ribosyltransferase, Vacuolating, and Receptor-Binding Activities

T. R. Kannan[1], **Manickam Krishnan**[1], **Kumaraguruparan Ramasamy**[1], **Argentina Becker**[2], **Olga N. Pakhomova**[2], **P. John Hart**[2,3], and **Joel B. Baseman**[1]

[1]Department of Microbiology and Immunology/Center for Airway Inflammation Research, The University of Texas Health Science Center at San Antonio, TX 78229

[2]Department of Biochemistry, The University of Texas Health Science Center at San Antonio, TX 78229

[3]Geriatric Research, Education, and Clinical Center, Department of Veterans Affairs, South Texas Veterans Health Care System, San Antonio TX, 78229

SUMMARY

Community-acquired respiratory distress syndrome (CARDS) toxin from *Mycoplasma pneumoniae* is a 591 amino acid virulence factor with ADP-ribosyltransferase (ADPRT) and vacuolating activities. It is expressed at low levels during *in vitro* growth and at high levels during colonization of the lung. Exposure of experimental animals to purified recombinant CARDS toxin alone is sufficient to recapitulate the cytopathology and inflammatory responses associated with *M. pneumoniae* infection in humans and animals. Here, by molecular modeling, serial truncations and site-directed mutagenesis, we show that the N-terminal region is essential for ADP-ribosylating activity. Also, by systematic truncation and limited proteolysis experiments we identified a portion of the C-terminal region that mediates toxin binding to mammalian cell surfaces and subsequent internalization. In addition, the C-terminal region alone induces vacuolization in a manner similar to full-length toxin. Together, these data suggest that CARDS toxin has a unique architecture with functionally separable N-terminal and C-terminal domains.

Keywords

ADP-ribosyltransferase; NAD-glycohydrolase; asthma; CARDS toxin; *Mycoplasma pneumoniae*; molecular modeling

Corresponding Authors: T.R. Kannan, Department of Microbiology & Immunology, UTHSCSA 78229, Tel: 210-562-4182; Fax: 210-562-4191; kannan@uthscsa.edu; Joel B. Baseman, Department of Microbiology & Immunology, UTHSCSA, 78229, Tel: 210-562-4190, Fax: 210-562-4191; baseman@uthscsa.edu.

INTRODUCTION

Mycoplasma pneumoniae is a bacterial pathogen that causes a broad range of human respiratory illnesses, including pharyngitis, tracheobronchitis, wheezing and community-acquired pneumonia (Atkinson *et al.*, 2008, Waites & Talkington, 2004). Evidence linking the organism to reactive airway diseases, such as asthma, is rapidly accumulating (Esposito *et al.*, 2000, Kraft, 2000, Biscardi *et al.*, 2004, Nisar *et al.*, 2007, Sutherland & Martin, 2007, Peters *et al.*, 2011). However, the airway is not the only target, as a spectrum of extra-pulmonary complications is also associated with *M. pneumoniae* infection (Baseman *et al.*, 1996, Talkington DF *et al.*, 2001, Berg *et al.*, 2009). *M. pneumoniae* pathogenicity depends on its attachment to, and colonization of the respiratory epithelium, and these processes are mediated by specific mycoplasma adhesins and adherence-accessory proteins (Baseman, 1993, Baseman et al., 1996).

While evaluating the potential of various host proteins to serve as targets of mycoplasma surface parasitism, a mycoplasma polypeptide designated as MPN372 was identified through its ability to bind surfactant protein-A, the major component of pulmonary surfactant (Kannan *et al.*, 2005). After MPN372 was found to possess ADP-ribosylating and vacuolating activities, it was designated Community-Acquired Respiratory Distress Syndrome (CARDS) toxin (Kannan & Baseman, 2006). In addition, CARDS toxin induces a robust inflammatory response with associated histopathology in baboon tracheal organ cultures and mouse bronchiolar epithelium (Kannan & Baseman, 2006, Hardy *et al.*, 2009).

This combination of biological activities suggests that CARDS toxin plays an important role in *M. pneumoniae* pathogenesis (Kannan & Baseman, 2006, Hardy et al., 2009). In support of this idea, CARDS toxin expression is dramatically limited during mycoplasma growth in laboratory media, in contrast to its markedly up-regulated synthesis during *M. pneumoniae* infection of the airway (Kannan *et al.*, 2010). CARDS toxin also elicits a strong immune response in convalescing humans and infected experimental animals and is readily detectable in airway fluids (Kannan et al., 2010, Techasaensiri *et al.*, 2010, Kannan *et al.*, 2011, Muir *et al.*, 2011, Peters et al., 2011, Kannan *et al.*, 2012). Furthermore, purified recombinant CARDS toxin elicits multiple inflammatory and temporally changing histopathological patterns in rodents and primates in a manner similar to those observed during *M. pneumoniae* infection (Hardy et al., 2009).

Sequence analyses indicate that CARDS toxin possesses amino acid sequence similarities to the catalytic subunit of the exotoxin from *Bordetella pertussis* (pertussis toxin; PT) (Kannan et al., 2005, Kannan & Baseman, 2006) and the catalytic domain of the exotoxin from *Vibrio cholerae* (cholera toxin; CT). Crystal structures and computer modeling studies of ADP-ribosyltransferase (ADPRT) toxins indicate that the N-terminal regions of specific ADPRTs, like pertussis, diphtheria, cholera, and heat-labile enterotoxin contain a conserved NAD-binding catalytic domain and a catalytic glutamate residue in their active sites, as does CARDS toxin. Unlike the catalytic PT S1 subunit (PT-S1) and the CT ADPRT subunits, which require additional subunits for binding and internalization (29), CARDS toxin, like diphtheria toxin (DT), is translated as a single polypeptide chain which binds to and is internalized by mammalian cells using clathrin-mediated pathways (Krishnan *et al.*, 2013).

Also, completely distinct from all other bacterial ADPRTs, CARDS toxin exhibits a striking vacuolating phenotype (Kannan & Baseman, 2006, Johnson *et al.*, 2011). Further, the C-terminal region of CARDS toxin shares no homology with any sequenced protein in the global database.

Here, we use structure prediction and molecular modeling combined with sequential deletion, site-directed mutagenesis and limited proteolysis to generate a series of soluble recombinant CARDS toxin variants that serve as functional probes to identify the molecular determinants of cell surface binding, vacuolating, and ADPRT activities. These data identify the minimal N-terminal region along with the amino acids necessary for ADPRT activity and the portion of the CARDS toxin molecule that enables host cell binding and internalization. Additionally, we show that the C-terminal region is essential for vacuolization.

RESULTS

Molecular Model of CARDS Toxin ADPRT Domain

The N-terminal region of CARDS toxin shares limited identity with the catalytic domain of many ADPRT toxins (Kannan & Baseman, 2006). To detect protein scaffolds compatible with the CARDS toxin amino acid sequence, we used the program HHPRED and the entire CARDS toxin amino acid sequence as the query. Table 1 shows the statistics for the five top-scoring hits of ADPRT domains of different toxins, which includes PT (Hazes *et al.*, 1996), typhoid toxin (Song *et al.*, 2013), CT (O'Neal *et al.*, 2005), LT (Sixma *et al.*, 1993), and mosquitocidal toxin (Reinert *et al.*, 2006). Since HHPRED predicted PT as the top structural template, we generated the molecular model of the CARDS toxin N-terminal region (residues 1–239) based on the PT structure using the program MODELLER (Sanchez & Sali, 1997, Sanchez & Sali, 2000) and subsequently superimposed the model on the structures of PT (Fig. 1A) and CT (Fig. 1B) ADPRT domains. The residues of the R---STS---E signature sequence expected to be involved in cofactor binding and catalysis are shown, as are several additional residues conserved in the active sites of the three toxins, including aspartic acid, arginine, and histidine residues (D12, R14, H36). The molecular model thus generated was subsequently compared to the structure of the CT ADPRT domain with NAD^+ bound [Fig. 1C; (O'Neal et al., 2005)]. Superposition of CARDS toxin ADPRT domain on CT (Fig. 1D) reinforces their close similarities during their interactions with NAD^+.

CARDS Toxin C-terminal Truncation Variants with ADPRT and NADase Activity

To identify and confirm the minimal N-terminal region essential for ADPRT activity, we constructed a series of C-terminal truncation variants of CARDS toxin by introducing stop codons within the coding region of UGA-corrected full length (FL) CARDS toxin at amino acid residues 186, 206, 228, 249, 307, 353, 391, 447, 507, 525 and 550 as indicated in Fig. S1-A. The parallel gel image shown in Fig. S1-B reveals that all of the expressed proteins migrate at their expected molecular masses. To cross-validate that the molecular determinants of ADPRT activity were housed within the N-terminal region, residues of the putative bacterial signature sequence were mutated to Ala. In addition to the conversion of

the putative E132 catalytic residue to alanine ($Glu^{132\rightarrow Ala}$) (Kannan & Baseman, 2006) we modified two other amino acid residues considered essential to ADPRT activity by converting arginine at position 10 and histidine at position 36 to alanine ($Arg^{10\rightarrow Ala}$ and $His^{36\rightarrow Ala}$, respectively) using overlap extension PCR (Fig. 2A).

To screen for ADPRT activity, we analyzed the C-terminal truncation variants (amino acids 1–206, 1–228, 1–249 and 1–550) and signature residue point mutants ($Arg^{10\rightarrow Ala}$, $His^{36\rightarrow Ala}$ and $Glu^{132\rightarrow Ala}$) for ADPRT activity (Fig. 2A). As indicated in Fig. 2B, all C-terminal truncation constructs retaining the ADPRT motif predicted in Fig. 1 catalyzed the ADP ribosylation of specific HeLa cell target proteins at ~50 kDa. C-terminal truncation variants smaller than the predicted motif exhibited lesser degrees of ADPRT activity (i.e., compare band intensities of truncation 1–249 to smaller truncations). In contrast, the three alanine-substituted purified CARDS toxin mutant proteins were individually tested for ADPRT activity and, as expected, none was observed, confirming that these amino acids are essential for ADP-ribosylation.

Since all ADP-ribosylating toxins also exhibit NAD glycohydrolase (NADase) activity in the absence of their specific ADP-ribose acceptor, we further defined the minimal CARDS toxin region with intact NADase activity using [carbonyl-^{14}C]NAD as described (Weng *et al.*, 1999). Like FL, all C-terminal truncation variants (amino acids 1–206, 1–228, 1–249 and 1–550) of CARDS toxin demonstrated NADase activity but to varying degrees. For example, using identical equimolar concentrations of FL and C-terminal truncations (140 pmoles), $CARDS_{249}$ exhibited NADase activity similar to FL toxin, whereas $CARDS_{206}$, $CARDS_{228}$ and $CARDS_{550}$ demonstrated 55%, 60% and 84% activities, respectively, relative to FL.

Binding and Internalization of CARDS Toxin Variants

To characterize the influence of modified ADPRT-related essential amino acids on binding and internalization of CARDS toxin, we labeled CARDS toxin and its derivatives with biotin. All three ADPRT CARDS toxin mutants ($Arg^{10\rightarrow Ala}$, $His^{36\rightarrow Ala}$ and $Glu^{132\rightarrow Ala}$; 10 μg/ml) exhibited comparable binding to FL CARDS toxin (data not shown). Furthermore, we incubated HeLa cell monolayers for 1h at 37°C with biotinylated $Arg^{10\rightarrow Ala}$, $His^{36\rightarrow Ala}$ and $Glu^{132\rightarrow Ala}$ mutant proteins and observed 96±5%, 97±7% and 93±6% internalization, respectively, when compared to FL toxin. As detected by immunofluorescence (Fig. 3), these mutant proteins exhibited similar internalization and distribution patterns in HeLa cells, like FL CARDS toxin. Fig. S2-A shows a schematic of FL CARDS toxin and the series of N-terminal CARDS toxin truncation variants tested for their cell surface receptor-binding and internalization capacities (amino acids 118–591, 178–591, 287–591, 366–591, 434–591, 466–591, and 516–591). The Nu-PAGE gel electrophoresis image shown in Fig. S2-B reveals that the expressed proteins migrate at their expected molecular masses. In this group, only CARDS toxin variants 118–591 and 178–591 were soluble and could be purified, while the remaining constructs were insoluble proteins.

FL CARDS toxin and truncation variants 1–249 ($CARDS_{249}$), 178–591($_{178}$CARDS), and 1–550 ($CARDS_{550}$) were biotinylated and tested for binding and internalization as described in Experimental Procedures. The results of the binding assay are shown in Fig. 4 and reveal

that truncation variants lacking the C-terminal region, including $CARDS_{550}$ which is missing the last 41 amino acids, fail to bind or be internalized. In contrast, the N-terminal truncation variant $_{178}$CARDS exhibited binding to HeLa cells similar to FL CARDS toxin [Fig. 4A; (Krishnan et al., 2013)] at 4°C. Upon shift to 37°C, the $_{178}$CARDS protein demonstrated internalization dynamics, like FL toxin (Fig. 4B). Immunofluorescence analysis confirmed the internalization of $_{178}$CARDS protein but not $CARDS_{550}$ (Fig. 4B) by HeLa cells.

Limited Proteolysis and Identification of Minimal Domain of CARDS Toxin Essential for Binding and Internalization

Since most of the N-terminal deletions yielded insoluble proteins, we used limited proteolysis to define the minimal region essential for binding and internalization. Limited protease digestion of FL CARDS toxin with trypsin or chymotrypsin yielded two distinct fragments of ~33 kDa and ~35 kDa, corresponding to cleavage on the C-terminal side of Lys305 and Lys307 (Pakhomova *et al.*, 2010). This process resulted in non-covalently associated domains defined by amino acid residues 1–305 and 308–591 (Fig. 5A). Attempts to purify the ~33 kDa protein (308–591) from the trypsin-digested FL CARDS toxin were unsuccessful due to an apparent strong association with the ~35 kDa N-terminal fragment. Furthermore, like most of the N-terminal truncated proteins, $_{308}$CARDS was unstable, even when using different *E. coli* vectors. Unlike FL CARDS toxin, chymotrypsin proteolysis of the $_{178}$CARDS protein yielded a soluble ~38 kDa fragment (Fig. 5A). However, at higher chymotrypsin concentrations (Fig. 5A), the ~38 kDa fragment was further digested to a ~33 kDa fragment, corresponding to $_{308}$CARDS. N-terminal sequencing of the ~38 kDa and ~33 kDa products indicated that they consist of residues 264–591 and 308–591, respectively (Fig. 5A).

Like FL CARDS toxin and $_{178}$CARDS, $_{264}$CARDS could be expressed in soluble form, and the purity and size of the protein were confirmed by SDS-PAGE (Fig. 5B). Comparison of biotin-labeled $_{264}$CARDS binding and internalization with FL CARDS toxin revealed that equimolar amounts of $_{264}$CARDS protein exhibited ~93±6% binding and 89±4% internalization relative to FL CARDS toxin. Immunofluorescence demonstrated that $_{264}$CARDS protein is internalized and distributed throughout the cytoplasm within 1 h (Fig. 5C) similar to FL (Fig. 3).

Dependence of Vacuolization on C-terminal Region of CARDS Toxin

All FL ADPRT signature sequence mutants of CARDS toxin were assayed for vacuolating activity. Under optimized buffer conditions, $Arg^{10\rightarrow Ala}$, $His^{36\rightarrow Ala}$ and $Glu^{132\rightarrow Ala}$ mutant proteins induced vacuolization, similar to FL CARDS toxin (data not shown). In addition, FL CARDS toxin exposed to limited trypsin proteolysis retained vacuolization activity (Fig. 6, see Discussion). When $_{178}$CARDS or $_{264}$CARDS proteins were incubated with HeLa cells, these truncation variants also induced vacuole formation, confirming the association between vacuolization and the C-terminal region (Fig. 6A). Interestingly, $_{178}$CARDS exhibited a diminished vacuolating phenotype compared to FL and other toxin derivatives (Fig 6B). Limited trypsin digestion of $_{178}$CARDS resulted in a C-terminal fragment (~33 kDa) corresponding to region 308–591 (Fig. 5A, $_{178}$CARDS panel, lane 2).

Like $_{264}$CARDS, the protease-cleaved $_{308}$CARDS also induced vacuole formation in HeLa cells (Fig. 6A–C). FL toxin (140 pmol) induced vacuole formation in all cells (100% within 12h), whereas cells treated with C-terminal derivatives (using the same molar concentrations as FL) exhibited varying degrees of vacuolization during the same 12h period. However, upon longer incubation (24–60h) all cells developed vacuoles, although the number and size of individual vacuoles varied (Fig. 6C).

DISCUSSION

Bacterial toxins modify targets in the cell cytosol or inner leaflet of the cytoplasmic membrane. ADP-ribosylating toxins damage or kill cells as a result of altered cell functions (Krueger & Barbieri, 1995, Locht & Antoine, 1995, Holbourn *et al.*, 2006, Kannan & Baseman, 2006, Deng & Barbieri, 2008). For this purpose, the classical ADP-ribosylating toxins typically retain at least three functional capabilities: 1) cell-surface receptor binding; 2) ability to translocate the ADPRT domain into the cytosol; and 3) ability to modify cellular protein targets by covalently attaching ADP-ribose to particular amino acids. These functions are often found in distinct domains of a single polypeptide chain (e.g., DT or Pseudomonas exotoxin A [PAETA]), or several protein chains (*e.g.*, PT or CT). Based on their conserved ‘S-X-S’ or ‘Y-(X)10-Y’ motif, ADP-ribosylating toxins are divided into two enzymatic groups: cholera toxin (CT)-like or diphtheria toxin (DT)-like, respectively (Domenighini & Rappuoli, 1996).

Identification of Minimal Soluble Domain Necessary for ADPRT Activity

As described earlier, analysis of the CARDS toxin amino acid sequence demonstrated the relationship between the N-terminal region of CARDS toxin (residues 1–239) and the catalytic subunit of the exotoxin from *B. pertussis* (Kannan et al., 2005). In contrast, residues 240–591 of CARDS toxin exhibited no detectable sequence similarity to any other protein in the non-redundant sequence database. We searched for possible structural homologs of CARDS toxin using pair-wise comparison of profile HMMs as implemented in the program HHPRED (Soding, 2005, Soding *et al.*, 2005) (see Experimental Procedures). CARDS toxin and PT residues are accounted for in both proteins using PT as the template (residues 3–230 of CARDS toxin are predicted to match residues 2–201 of PT, see Table 1). The high degree of structural similarity between the molecular model of the CARDS toxin ADPRT domain with those of PT and CT in the protein data bank [pdb codes 1bcp (Hazes et al., 1996) and 1s5d (O'Neal *et al.*, 2004), respectively] is evident in Figs. 1A and 1B. All three proteins have the signature sequence R---STS---E and histidine with the modeled CT possessing the only difference - an Asp instead of a Glu in the position identified as a key acidic residue necessary for catalysis. Comparison of the CARDS toxin active site model with the structure of the CT active site shown in Fig. 1C and 1D reveals that the two proteins possess essentially identical residues poised to interact with NAD^+, with Arg14, Asp12, and Arg10 in CARDS toxin analogous to Arg11, Asp9, and Arg 7 of CT. The slight differences in position of the various side chains arise because CARDS toxin side chains are not constrained by contact with cofactor during the satisfaction of spatial restraints calculation in MODELLER (Sanchez & Sali, 1997, Sanchez & Sali, 2000). In addition to the conversion of the putative E132 catalytic residue to alanine ($Glu^{132\rightarrow Ala}$) reported earlier

(Kannan & Baseman, 2006), converting arginine at position 10 and histidine at position 36 to alanine ($Arg^{10\rightarrow Ala}$ and $His^{36\rightarrow Ala}$) abolished the ADPRT activity, confirming that these amino acids are essential for ADP-ribosylation.

The catalytic glutamic acid residue at position 132 in CARDS toxin [analogous to Glu148 of DT Glu553 of PAETA, Glu112 of CT and LT, Glu129 of PT, and Glu214 of *Clostridium botulinum* C3 exoenzyme] is similar to the well characterized Glu/Gln-X-Glu motif characteristic of the CT group. The other conserved amino acids considered important in catalysis are CARDS toxin Arg 10 [equivalent to Arg 9 of PT (Burnette *et al.*, 1988) and Arg 7 of CT or LT (Burnette *et al.*, 1991, Lobet *et al.*, 1991)] and His36 [equivalent to His35 of PT (Xu *et al.*, 1994), His 44 of LT (Kato *et al.*, 1997) and CT (Jobling & Holmes, 2001)]. CARDS toxin Glu132 likely stabilizes a chemical intermediate of NAD^+ by forming a hydrogen bond with the O_2' hydroxyl group of the nicotinamide ribose (Han *et al.*, 1999). Except for pertussis and cholera toxins, the predicted α-β structure of CARDS toxin has minimal amino acid sequence identity to other ADP-ribosylating toxins. However, it retains the consensus STS, which is predicted to reside in a β-strand 3 that serves as the "floor" of the cavity in most of the enzymes of the CT group in which NAD^+ binds (Domenighini & Rappuoli, 1996). Because of the observed ADPRT activities of FL and truncated toxins (Fig 2B), we compared these proteins for NADase activities using equimolar concentrations of FL and C-terminal truncation variants. Like ADPRT levels, we detected similar patterns of enzymatic activities, suggesting that amino acid residues between 228 and 249 are critical to maintain both ADPRT and NADase activities and/or proper conformation of the active site.

Receptor Binding and Vacuolating Activities of CARDS Toxin

Although the *M. pneumoniae* CARDS toxin ADPRT domain is structurally similar to the PT-S1 and CT catalytic subunits, CARDS toxin does not possess the pentameric arrangement of peptide chains that act in receptor binding and internalization in those toxins. Instead, the single peptide organization of CARDS toxin is more similar to the DT group of toxins, like DT and PAETA. Deletion of the C-terminal region of CARDS toxin completely abrogated its binding and internalization, suggesting that the C-terminus performs a role analogous to the pentameric assembly of PT-S1 and CT (Fig 4A–C). Removal of the last 41 amino acids from the C-terminal end of CARDS toxin (residues 551–591) abolishes binding, indicating that this region directly mediates binding to host cell membrane receptor(s) or that deletion of this region alters the local conformation of CARDS toxin, thereby preventing toxin-receptor interactions.

Although most of the N-terminal truncation variant constructs of CARDS toxin resulted in insoluble recombinant proteins, $_{178}$CARDS and $_{264}$CARDS truncations and protease-released $_{308}$CARDS peptide yielded soluble proteins (Figs. S2 and Fig. 5). Their availability as reagents enabled us to demonstrate that the C-terminal region is responsible for binding and internalization. In addition, the vacuolating properties of CARDS toxin were directly associated with the C-terminal domain, demonstrating that the CARDS toxin C-terminus possesses functions beyond cell-surface binding and internalization (Fig. 6). Further, decreased vacuolization was detected with all N-terminal truncations, when compared to FL, suggesting a possible role of the N-terminal region in maintaining conformational integrity

of the C-terminal region. The vacuolization induced by bacterial toxins has been examined in the case of cytotoxin VacA from *Helicobacter pylori* (Cover & Blaser, 1992) and AB5 subtilase cytotoxin (SubAB) of Shiga-toxigenic *E. coli* (Paton *et al.*, 2004). Similar to the CARDS toxin C-terminal binding region, the B domain of SubAB toxin causes vacuolation (Morinaga *et al.*, 2007). However, no sequence similarity between CARDS toxin and the functional vacuolating domains of VacA and SubAB has been identified, which could explain differences observed in the vacuole phenotype generated by CARDS toxin versus VacA (Johnson et al., 2011, Papini *et al.*, 1994).

Parallels between CARDS toxin and DT via Intramolecular "Nicking"

Because CARDS toxin and DT are both translated as single polypeptide chains, comparisons between them are of special interest. When DT is cleaved by trypsin, the A-fragment remains linked by a disulfide bond to the B-fragment (Pappenheimer, 1977). In previous work (Pakhomova et al., 2010), we observed that limited proteolysis of FL CARDS toxin with trypsin or chymotrypsin resulted in cleavage on the C-terminal side of Lys305 and/or Lys307 to yield two distinct fragments of ~33 kDa and ~35 kDa. Since both protease-released fragments remained strongly associated with each other, even after digestion, purification of the ~33 kDa fragment (308–591) from the trypsin-digested CARDS toxin was unsuccessful. This ‘nicked’ CARDS protein, upon addition to mammalian cells, exhibited binding and internalization similar to FL CARDS toxin (Fig. 7A and B). Expression of the 308–591 fragment as a recombinant protein in *E. coli* did not yield a soluble protein. However, the limited trypsin digestion of $_{178}$CARDS resulted in a C-terminal fragment corresponding to amino acid sequence 308–591 (Fig. 5, $_{178}$CARDS panel lane 2). This $_{308}$CARDS fragment, when purified by size exclusion column chromatography, remained soluble at pH 8.0 and, like $_{178}$CARDS and $_{264}$CARDS, induced vacuolization. As expected, CARDS$_{249}$ which possessed the key ADP-ribosylating N-terminal region, but lacked the C-terminal region, failed to induce vacuolization. These data clearly establish the C-terminus of CARDS toxin as the mediator of vacuolization (Fig. 8).

Altogether, our results strongly suggest that the ADPRT domain of CARDS toxin is similar to other CT group toxins. However, the C-terminal region is unique, consisting of a cell binding and internalization domain with vacuolating activity. This latter region may also play a decisive role in the translocation of the A-fragment to the cytosol and to specific organelles. Additional studies to identify transcytosis and trafficking pathways will help to clarify the mechanisms of toxin action at the cellular and molecular levels and assist in expanding the role of CARDS toxin as a bona fide virulence determinant and therapeutic target of *M. pneumoniae*.

EXPERIMENTAL PROCEDURES

Bacterial Strains and Mammalian Cell Culture Conditions

Escherichia coli TOP10 (Invitrogen) and *E. coli* BL21(DE3) (Stratagene) were grown in Luria-Bertani (LB) broth. HeLa cells (CCL-2) were obtained from the American Type Culture Collection (ATCC) and grown in minimal essential medium (MEM) supplemented with 10% fetal bovine serum (FBS) (Atlas Biologicals). All cell cultures were grown under

air-5% CO_2 at 37°C and routinely certified to be free of mycoplasma contamination (MycoProbe Mycoplasma detection kit [R&D Systems]).

Cloning, Site-directed Mutagenesis, Expression, and Purification of CARDS Toxin Variants

Plasmid DNA containing the TGA-corrected FL CARDS toxin gene sequence was purified using the QIAprep spin protocol according to the manufacturer's instructions (Qiagen). Gene fragments were amplified by PCR using TGA-corrected CARDS toxin DNA as a template. Site-directed mutagenesis of amino acids in the N-terminal ADP ribosyltransferase domain was achieved by overlap extension PCR as described previously using the primers indicated in Table 1 (Ho *et al.*, 1989). Varying lengths of the C-terminal coding region were deleted by introducing stop codons within the open reading frame. PCR products of variable lengths of the C-terminal coding region were generated and cloned into pCR2.1, which were subsequently digested with NdeI and BamHI and ligated into pET19b or pKA8H. The latter is an expression vector with a tobacco etch virus (TEV) protease cleavable site between the His tag and the N-terminus of CARDS toxin derivatives. These plasmids were transformed into competent *E. coli* BL21(DE3), and recombinant colonies were screened for resistance to ampicillin and expression of variable CARDS toxin proteins. Verification of each construct was achieved by complete DNA sequencing of individual plasmids (Department of Microbiology and Immunology *Nucleic Acids Core Facility*, University of Texas Health Science Center at San Antonio). Induction of recombinant protein synthesis in *E. coli* was achieved by the addition of 40–100 μM isopropyl-β-d-thiogalactopyranoside (IPTG; Sigma-Aldrich) and bacteria were incubated for 4 h at 37°C under aeration at 210 rpm or overnight at varying temperatures ranging between 25°C to 18°C. Fusion proteins were purified by nickel affinity chromatography under native conditions or under denatured conditions (Qiagen). All recombinant proteins were desalted in 50 mM Tris-HCl buffer (pH 8.0) plus 5% glycerol using PD-10 columns, and protein purity was assessed by SDS-PAGE. Recombinant proteins produced in *E. coli* as inclusion bodies were purified and renatured using dialysis and gel filtration in a Sepharose CL-6B column (GE Healthcare).

Structure Prediction and Molecular Modeling

To identify the sequence elements of CARDS toxin that correspond to ADPRT and vacuolating activities, we searched the protein data bank (PDB) for structural homologs using the program HHPRED (Soding, 2005, Soding et al., 2005). HHPRED detects remote protein homology and predicts protein structure using pairwise comparisons of profile hidden Markov models (HMMs). Briefly, a multiple sequence alignment was constructed for the CARDS toxin sequence through multiple iterations of PSI-BLAST against the non-redundant sequence database from NCBI. Second, a single CARDS toxin profile HMM was generated from this multiple sequence alignment, which contains a statistical description of the alignment, including secondary structural information. For each column in the multiple sequence alignment that has a residue in the query sequence, an HMM column was created that contains the probabilities of each of the 20 amino acids plus four probabilities that describe how often amino acids were inserted and deleted at this position (insert open and extend and delete open and extend). These insert/delete probabilities were translated into position-specific gap penalties when an HMM is aligned to a sequence or to another HMM (Soding, 2005, Soding et al., 2005). These same procedures were pre-calculated for each

sequence corresponding to a known structure in the PDB in order to generate a library of profile HMMs to which the query profile HMM can be rapidly compared. Third, the query profile HMM was compared to each profile HMM in the structural database and scored (Soding, 2005, Soding et al., 2005). The HHPRED output, which consists of an alignment of a sequence to be modeled with known related structures, was used as input for the program MODELLER, which automatically calculates a model of the query sequence containing all non-hydrogen atoms by satisfaction of spatial restraints (Sanchez & Sali, 1997, Sanchez & Sali, 2000). All images depicting protein structures and molecular models were created in the program PyMol (The PyMOL Molecular Graphics System, Version 1.5.0.4 Schrödinger, LLC.)

Protease Digestion and Purification of CARDS Toxin C-terminal Region

Purified FL CARDS toxin and N-terminal truncation $_{178}$CARDS protein were digested with trypsin and chymotrypsin (Pakhomova et al., 2010). Briefly, purified proteins in storage buffer at 1 mg mL^{-1} were incubated with different concentrations of trypsin or chymotrypsin (100, 50, 25, 20, 10 or 1 μg) for 30 min at room temperature. Proteolysis was terminated by adding PMSF (100 μM; Fluka). Resultant preparations were filtered through 0.2 μm syringe filters and loaded onto Sephacryl S-100 HR 16/60 or Superdex 75 10/300 GL columns (GE Healthcare) equilibrated with 50mM Tris–HCl pH 8.0. Proteins were eluted with the same buffer at a flow rate of 0.5mL/min.

N-terminal Sequencing

PVDF membrane (Immobilion P; Millipore) blots of SDS-polyacrylamide gels containing protease-digested FL CARDS toxin or $_{178}$CARDS protein bands were excised from blots and subjected to Edman degradation sequencing by the N-terminal protein sequencing facility at Midwest Analytical Inc. (St. Louis, MO).

Quantification of Proteins and Nucleic Acids

Protein concentrations were estimated by the bicinchoninic acid method (Pierce, Rockford, IL) with bovine serum albumin (BSA) as a standard. DNA, RNA, and purified plasmid sample concentrations were assayed at 260 nm using a NanoDrop ND-1000 spectrophotometer (Thermo Scientific).

Binding and Internalization of CARDS Toxin and its Derivatives

Binding and internalization of CARDS toxin and its derivatives were analyzed as we earlier reported (Krishnan et al., 2013). In brief, HeLa cells (5×10^4 cells/well) were cultured in Eagle's MEM medium with 10% fetal calf serum in 96-well plates overnight at 37°C. Biotin-labeled CARDS toxin and its derivatives were prepared according to the manufacturer's instructions, using EZ-Link sulfo-*N*-hydroxylsulfosuccinimide-biotin (sulfo-NHS-SS-biotin) (Pierce USA). For binding studies, monolayers of HeLa cells were treated with biotin-labeled FL CARDS toxin or its derivatives (140 pmol) in HBSS-BSA at 4°C for 60 min, and the bound proteins were analyzed using horseradish peroxidase (HRP)-conjugated streptavidin (Pierce, USA). Color intensity was measured at 450 nm using ELISA reader (MRX Dynatech Lab., USA) as previously described (Krishnan et al., 2013).

For internalization studies, biotin-labeled FL CARDS toxin or its derivatives were added to monolayers at 4°C for 1h. The temperature was shifted to 37°C, and incubation was continued for 60 min. Cells were subjected to 2-mercaptoethanesulfonic acid (0.5M) to remove cell surface-bound biotin. Then, cells were permeabilized, and internalized biotin-labeled proteins were estimated using HRP-conjugated streptavidin (Krishnan et al., 2013).

ADPRT Assay

ADPRT activity of CARDS toxin and its derivatives was performed as previously described (Kannan & Baseman, 2006). Briefly, HeLa cells were grown to 80% confluence, washed, harvested, and sonicated in 50 mM Tris (pH 7.4). HeLa cell lysates were incubated with FL CARDS toxin and its derivatives in a 50-μl reaction mixture volume of 10 mM thymidine (Sigma), 10 mM dithiothreitol (Sigma), 2.5 mM $MgCl_2$ (Sigma), 50 mM Tris (pH 7.4), and 0.2 μM [^{32}P]NAD (800 Ci/mmol; Perkin-Elmer). Fifty-microliter reaction mixture volumes were incubated at 30°C for 30 min, trichloroacetic acid (Sigma) precipitated, and spun at 16,000 × g for 10 min. Cell pellets were dissolved in NuPAGE sample buffer (Invitrogen) and run on NuPAGE 4 to 12% Bis-Tris gradient gels (Invitrogen) for 60 min at 200 V. Gels were transferred onto 0.2-μm nitrocellulose membranes (Protran BA83; Schleicher & Schuell) for 1 h at 15 V and Ponceau (Sigma) stained to determine efficient protein transfer. Membranes were exposed to autoradiographic films (Kodak) for 1 day to 1 week at −80°C and developed.

NADase Assay

NADase activity of CARDS toxin and its variants was analyzed as previously described by Weng et.al., with a slight modification (Weng et al., 1999). In brief, 300 μl of reaction mixture containing 50 mM potassium phosphate (pH 7.5), equimolar concentrations of FL and N-terminal variants of CARDS toxin (140 or 700 pmol), 100 mM dithiothreitol, 1mg/ml BSA, 0.1 mM [carbonyl-^{14}C]NAD (0.05 μCi, PerkinElmer) were incubated at 30°C for 2–6 h. After incubation, samples (100 μl) were applied to columns (0.8 X 4 cm) of AG1-X2 (Bio-Rad), equilibrated, and eluted with 5 X 1 mL of water, and radioactivity was quantified (Beckman LS 6500 liquid scintillation counter). Pertussis toxin A promoter (List Biologicals Laboratories, Inc.) was used as a positive control to establish validity of the NADase assay.

Vacuolization Assessment

Monolayers of HeLa cells were grown to 50 to 60% confluence in 25-cm^2 flasks in MEM (ATCC) supplemented with 10% FBS (Atlas Biologicals) at 37°C and air-5% CO_2. Depleted culture medium was replaced by fresh MEM without serum, and FL CARDS toxin and its variants (140, 350 and 700 pmoles) were added. After 1 h at 37°C, HeLa cells were incubated in the presence or absence of 10% FBS and analyzed for vacuolization for up to 60 h. HeLa cells with carrier buffer solution served as negative controls. The number of vacuoles per cell and the number of vacuolated cells per field were recorded at different time points. All experiments were repeated in triplicate, and 10 fields of 20–25 cells per sample were examined to determine the vacuolization patterns. Statistical analysis was performed using Microsoft Excel.

Immunofluorescence Microscopy Analysis

HeLa cells were seeded at 1×10^5 cells/well in 24-well plates (Corning) on glass coverslips (1.5 μm; Fisher Scientific) at 37°C in air-5% CO_2 for 24 h before intoxication. Cells were treated with 10 μg mL^{-1} of FL CARDS toxin or its engineered variants and incubated for 1 h at 37°C in air-5% CO_2. Cells were washed in PHEM buffer (60 mM PIPES, 25 mM HEPES, 2 mM EGTA and 10 mM $MgCl_2$ pH7.2), fixed in 2% paraformaldehyde (Electron Microscopy Sciences) for 20 min, permeabilized with 0.1% Triton X-100 for 10 min and blocked with 5% normal goat serum (NGS) in PHEM buffer. Then, cells were incubated with rabbit polyclonal anti-CARDS toxin antibody (1:1000) for 1 h in PBS-0.2% NGS, washed, and incubated with goat anti-rabbit Alexa Fluor 633 antibody (Invitrogen) in PBS-0.2% NGS for 1 h. Individual coverslips were washed in PBS and mounted with Vectashield-1500 with DAPI (4′,6′-diamidino-2-phenylindole dihydrochloride). Cells without CARDS toxin were processed similarly to serve as negative controls. Coverslips were sealed with clear nail polish to prevent drying and movement under the microscope. All samples were examined using an Olympus XI-81 confocal laser scanning microscope with Flow view 1000 imaging software.

Supplementary Material

Refer to Web version on PubMed Central for supplementary material.

Acknowledgments

We thank Tiffany McDonald Marsh, Pramod Gowda, Brandon Guin and Dr. Sowmya Balasubramanian for their technical assistance. We would like to thank Rose Garza for assembling the manuscript. This work was supported by Award Number U19AI070412 from the National Institute of Allergy and Infectious Diseases, The Kleberg Foundation, and the Robert A. Welch Foundation grant AQ-1399 (PJH). The content is solely the responsibility of the authors and does not necessarily represent the official views of the National Institute of Allergy and Infectious Diseases or the National Institutes of Health. This work is partially the result of research conducted at the Northeastern Collaborative Access Team (NE-CAT) beam lines of the Advanced Photon Source, supported by award RR-15301 from the National Center for Research Resources at the National Institute of Health. Use of the Advanced Photon Source is supported by the U.S. Department of Energy, Office of Basic Energy Sciences, under contract No. W-31-109-ENG-38. This work was also supported in part by the Cancer Therapy & Research Center (CTRC) Cancer Center Support Grant, NCI P30CA054174 and support for the *X-ray Crystallography Core Laboratory* by the UTHSCSA Executive Research Committee is gratefully acknowledged.

REFERENCES

Atkinson TP, Balish MF, Waites KB. Epidemiology, clinical manifestations, pathogenesis and laboratory detection of *Mycoplasma pneumoniae* infections. FEMS Microbiol Rev. 2008; 32:956–973. [PubMed: 18754792]

Baseman JB. The cytadhesins of *Mycoplasma pneumoniae* and *M genitalium* . Subcell Biochem. 1993; 20:243–259. [PubMed: 8378992]

Baseman JB, Reddy SP, Dallo SF. Interplay between mycoplasma surface proteins, airway cells, and the protean manifestations of mycoplasma-mediated human infections. Am J Respir Crit Care Med. 1996; 154:S137–S144. [PubMed: 8876532]

Berg CP, Kannan TR, Klein R, Gregor M, Baseman JB, Wesselborg S, Lauber K, Stein GM. Mycoplasma antigens as a possible trigger for the induction of antimitochondrial antibodies in primary biliary cirrhosis. Liver Int. 2009; 29:797–809. [PubMed: 19638108]

Biscardi S, Lorrot M, Marc E, Moulin F, Boutonnat-Faucher B, Heilbronner C, Iniguez JL, Chaussain M, Nicand E, Raymond J, Gendrel D. *Mycoplasma pneumoniae* and asthma in children. Clin Infect Dis. 2004; 38:1341–1346. [PubMed: 15156467]

Burnette WN, Cieplak W, Mar VL, Kaljot KT, Sato H, Keith JM. Pertussis toxin S1 mutant with reduced enzyme activity and a conserved protective epitope. Science. 1988; 242:72–74. [PubMed: 2459776]

Burnette WN, Mar VL, Platler BW, Schlotterbeck JD, McGinley MD, Stoney KS, Rohde MF, Kaslow HR. Site-specific mutagenesis of the catalytic subunit of cholera toxin: substituting lysine for arginine 7 causes loss of activity. Infect Immun. 1991; 59:4266–4270. [PubMed: 1937784]

Cover TL, Blaser MJ. Purification and characterization of the vacuolating toxin from *Helicobacter pylori* . The Journal of biological chemistry. 1992; 267:10570–10575. [PubMed: 1587837]

Deng Q, Barbieri JT. Molecular mechanisms of the cytotoxicity of ADP-ribosylating toxins. Annu Rev Microbiol. 2008; 62:271–288. [PubMed: 18785839]

Domenighini M, Rappuoli R. Three conserved consensus sequences identify the NAD-binding site of ADP-ribosylating enzymes, expressed by eukaryotes, bacteria and T-even bacteriophages. Mol Microbiol. 1996; 21:667–674. [PubMed: 8878030]

Esposito S, Blasi F, Arosio C, Fioravanti L, Fagetti L, Droghetti R, Tarsia P, Allegra L, Principi N. Importance of acute *Mycoplasma pneumoniae* and *Chlamydia pneumoniae* infections in children with wheezing. Eur Respir J. 2000; 16:1142–1146. [PubMed: 11292120]

Han S, Craig JA, Putnam CD, Carozzi NB, Tainer JA. Evolution and mechanism from structures of an ADP-ribosylating toxin and NAD complex. Nat Struct Biol. 1999; 6:932–936. [PubMed: 10504727]

Hardy RD, Coalson JJ, Peters J, Chaparro A, Techasaensiri C, Cantwell AM, Kannan TR, Baseman JB, Dube PH. Analysis of pulmonary inflammation and function in the mouse and baboon after exposure to *Mycoplasma pneumoniae* CARDS toxin. PLoS One. 2009; 4:e7562. [PubMed: 19859545]

Hazes B, Boodhoo A, Cockle SA, Read RJ. Crystal structure of the pertussis toxin-ATP complex: a molecular sensor. Journal of molecular biology. 1996; 258:661–671. [PubMed: 8637000]

Ho SN, Hunt HD, Horton RM, Pullen JK, Pease LR. Site-directed mutagenesis by overlap extension using the polymerase chain reaction. Gene. 1989; 77:51–59. [PubMed: 2744487]

Holbourn KP, Shone CC, Acharya KR. A family of killer toxins. Exploring the mechanism of ADP-ribosylating toxins. FEBS J. 2006; 273:4579–4593. [PubMed: 16956368]

Jobling MG, Holmes RK. Biological and biochemical characterization of variant A subunits of cholera toxin constructed by site-directed mutagenesis. J Bacteriol. 2001; 183:4024–4032. [PubMed: 11395467]

Johnson C, Kannan TR, Baseman JB. Cellular vacuoles induced by *Mycoplasma pneumoniae* CARDS toxin originate from Rab9-associated compartments. PLoS One. 2011; 6:e22877. [PubMed: 21829543]

Kannan TR, Baseman JB. ADP-ribosylating and vacuolating cytotoxin of *Mycoplasma pneumoniae* represents unique virulence determinant among bacterial pathogens. Proc Natl Acad Sci U S A. 2006; 103:6724–6729. [PubMed: 16617115]

Kannan TR, Coalson JJ, Cagle M, Musatovova O, Hardy RD, Baseman JB. Synthesis and distribution of CARDS toxin during *Mycoplasma pneumoniae* infection in a murine model. J Infect Dis. 2011; 204:1596–1604. [PubMed: 21957154]

Kannan TR, Hardy RD, Coalson JJ, Cavuoti DC, Siegel JD, Cagle M, Musatovova O, Herrera C, Baseman JB. Fatal outcomes in family transmission of *Mycoplasma pneumoniae* . Clin Infect Dis. 2012; 54:225–231. [PubMed: 22052890]

Kannan TR, Musatovova O, Balasubramanian S, Cagle M, Jordan JL, Krunkosky TM, Davis A, Hardy RD, Baseman JB. *Mycoplasma pneumoniae* Community Acquired Respiratory Distress Syndrome toxin expression reveals growth phase and infection-dependent regulation. Mol Microbiol. 2010; 76:1127–1141. [PubMed: 20199607]

Kannan TR, Provenzano D, Wright JR, Baseman JB. Identification and characterization of human surfactant protein A binding protein of *Mycoplasma pneumoniae* . Infect Immun. 2005; 73:2828–2834. [PubMed: 15845487]

Kato M, Imamura S, Kawase H, Miyama A, Tsuji T. Histidine-44 of the A subunit of *Escherichia coli* enterotoxin is involved in its enzymatic and biological activities. FEMS Microbiol Lett. 1997; 152:219–225. [PubMed: 9231414]

Kraft M. The role of bacterial infections in asthma. Clin Chest Med. 2000; 21:301–313. [PubMed: 10907590]

Krishnan M, Kannan TR, Baseman JB. *Mycoplasma pneumoniae* CARDS toxin is internalized via clathrin-mediated endocytosis. PLoS One. 2013; 8:e62706. [PubMed: 23667510]

Krueger KM, Barbieri JT. The family of bacterial ADP-ribosylating exotoxins. Clin Microbiol Rev. 1995; 8:34–47. [PubMed: 7704894]

Lobet Y, Cluff CW, Cieplak W Jr. Effect of site-directed mutagenic alterations on ADP-ribosyltransferase activity of the A subunit of *Escherichia coli* heat-labile enterotoxin. Infect Immun. 1991; 59:2870–2879. [PubMed: 1908825]

Locht C, Antoine R. A proposed mechanism of ADP-ribosylation catalyzed by the pertussis toxin S1 subunit. Biochimie. 1995; 77:333–340. [PubMed: 8527486]

Morinaga N, Yahiro K, Matsuura G, Watanabe M, Nomura F, Moss J, Noda M. Two distinct cytotoxic activities of subtilase cytotoxin produced by shiga-toxigenic *Escherichia coli* . Infect Immun. 2007; 75:488–496. [PubMed: 17101670]

Muir MT, Cohn SM, Louden C, Kannan TR, Baseman JB. Novel toxin assays implicate *Mycoplasma pneumoniae* in prolonged ventilator course and hypoxemia. Chest. 2011; 139:305–310. [PubMed: 20884727]

Nisar N, Guleria R, Kumar S, Chand Chawla T, Ranjan Biswas N. *Mycoplasma pneumoniae* and its role in asthma. Postgrad Med J. 2007; 83:100–104. [PubMed: 17308212]

O'Neal CJ, Amaya EI, Jobling MG, Holmes RK, Hol WG. Crystal structures of an intrinsically active cholera toxin mutant yield insight into the toxin activation mechanism. Biochemistry. 2004; 43:3772–3782. [PubMed: 15049684]

O'Neal CJ, Jobling MG, Holmes RK, Hol WG. Structural basis for the activation of cholera toxin by human ARF6-GTP. Science. 2005; 309:1093–1096. [PubMed: 16099990]

Pakhomova ON, Taylor AB, Becker A, Holloway SP, Kannan TR, Baseman JB, Hart PJ. Crystallization of community-acquired respiratory distress syndrome toxin from *Mycoplasma pneumoniae* . Acta Crystallogr Sect F Struct Biol Cryst Commun. 2010; 66:294–296.

Papini E, de Bernard M, Milia E, Bugnoli M, Zerial M, Rappuoli R, Montecucco C. Cellular vacuoles induced by *Helicobacter pylori* originate from late endosomal compartments. Proc Natl Acad Sci U S A. 1994; 91:9720–9724. [PubMed: 7937879]

Pappenheimer AM Jr. Diphtheria toxin. Annu Rev Biochem. 1977; 46:69–94. [PubMed: 20040]

Paton AW, Srimanote P, Talbot UM, Wang H, Paton JC. A new family of potent AB(5) cytotoxins produced by Shiga toxigenic *Escherichia coli* . J Exp Med. 2004; 200:35–46. [PubMed: 15226357]

Peters J, Singh H, Brooks EG, Diaz J, Kannan TR, Coalson JJ, Baseman JG, Cagle M, Baseman JB. Persistence of community-acquired respiratory distress syndrome toxin-producing *Mycoplasma pneumoniae* in refractory asthma. Chest. 2011; 140:401–407. [PubMed: 21622549]

Reinert DJ, Carpusca I, Aktories K, Schulz GE. Structure of the mosquitocidal toxin from *Bacillus sphaericus* . Journal of molecular biology. 2006; 357:1226–1236. [PubMed: 16483607]

Sanchez R, Sali A. Evaluation of comparative protein structure modeling by MODELLER-3. Proteins. 1997; (Suppl 1):50–58. [PubMed: 9485495]

Sanchez R, Sali A. Comparative protein structure modeling. Introduction and practical examples with modeller. Methods in molecular biology. 2000; 143:97–129. [PubMed: 11084904]

Sixma TK, Kalk KH, van Zanten BA, Dauter Z, Kingma J, Witholt B, Hol WG. Refined structure of *Escherichia coli* heat-labile enterotoxin, a close relative of cholera toxin. Journal of molecular biology. 1993; 230:890–918. [PubMed: 8478941]

Soding J. Protein homology detection by HMM-HMM comparison. Bioinformatics. 2005; 21:951–960. [PubMed: 15531603]

Soding J, Biegert A, Lupas AN. The HHpred interactive server for protein homology detection and structure prediction. Nucleic acids research. 2005; 33:W244–W248. [PubMed: 15980461]

Song J, Gao X, Galan JE. Structure and function of the *Salmonella* Typhi chimaeric A_2B_5 typhoid toxin. Nature. 2013; 499:350–354. [PubMed: 23842500]

Sutherland ER, Martin RJ. Asthma and atypical bacterial infection. Chest. 2007; 132:1962–1966. [PubMed: 18079229]

Talkington, DF.; Waites, KB.; Schwartz, SB.; RE, B. Emerging from obscurity: understanding pulmonary and extrapulmonary syndromes, pathogenesis, and epidemiology of human *Mycoplasma pneumoniae* infections. In: Scheld, WM.; Craig, WA.; JM, H., editors. Emerging infections. Washington, DC: American Society for Microbiology; 2001. p. 57-84.

Techasaensiri C, Tagliabue C, Cagle M, Iranpour P, Katz K, Kannan TR, Coalson JJ, Baseman JB, Hardy RD. Variation in colonization, ADP-ribosylating and vacuolating cytotoxin, and pulmonary disease severity among *Mycoplasma pneumoniae* strains. Am J Respir Crit Care Med. 2010; 182:797–804. [PubMed: 20508214]

Waites KB, Talkington DF. *Mycoplasma pneumoniae* and its role as a human pathogen. Clin Microbiol Rev. 2004; 17:697–728. [PubMed: 15489344]

Weng B, Thompson WC, Kim HJ, Levine RL, Moss J. Modification of the ADP-ribosyltransferase and NAD glycohydrolase activities of a mammalian transferase (ADP-ribosyltransferase 5) by auto-ADP-ribosylation. The Journal of biological chemistry. 1999; 274:31797–31803. [PubMed: 10542202]

Xu Y, Barbancon-Finck V, Barbieri JT. Role of histidine 35 of the S1 subunit of pertussis toxin in the ADP-ribosylation of transducin. The Journal of biological chemistry. 1994; 269:9993–9999. [PubMed: 8144593]

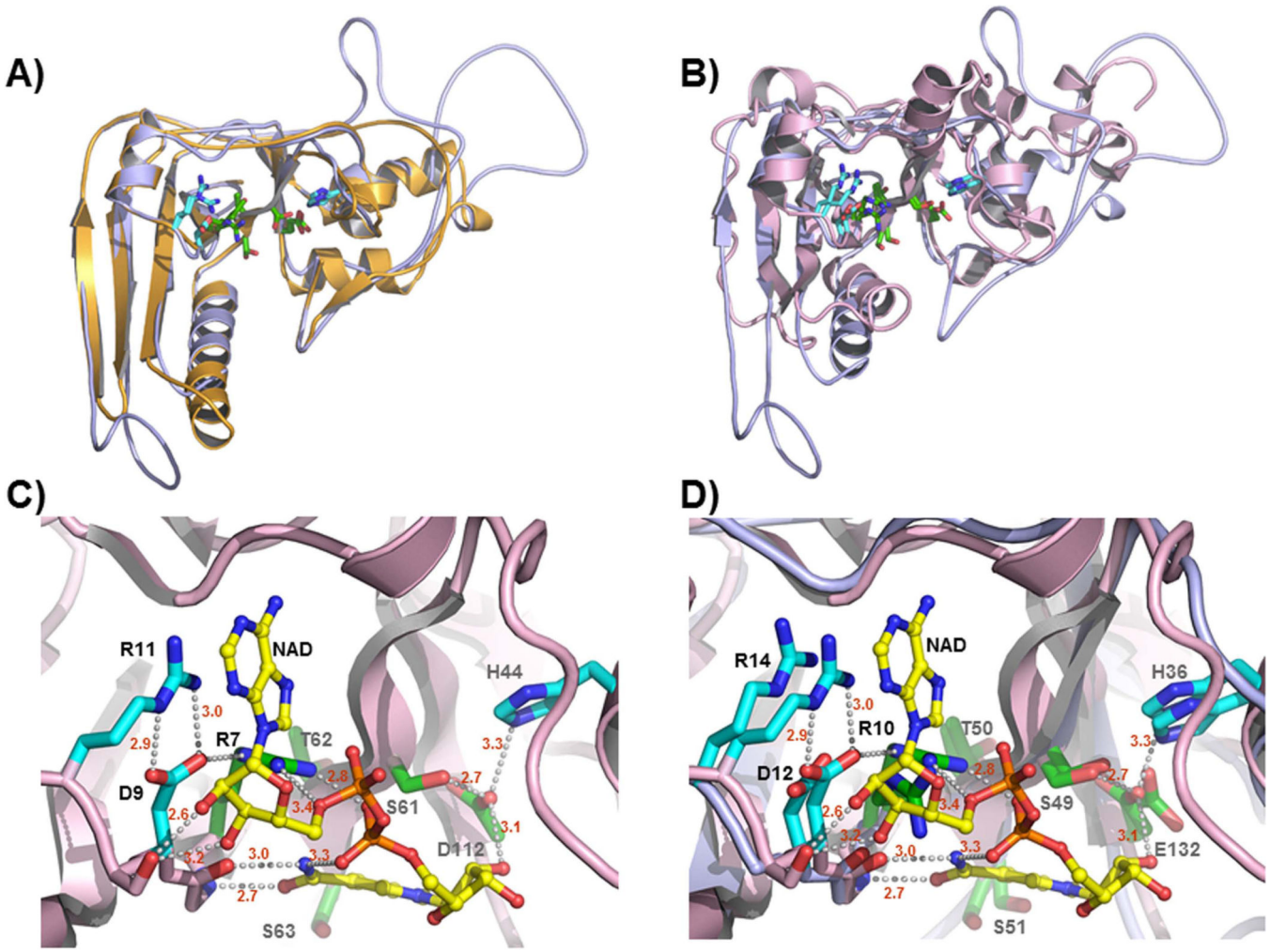

Fig. 1. Molecular model of CARDS toxin ADPRT domain reveals spatial conservation of the bacterial ADPRT signature motif and suggests a conserved mode of NAD$^+$ binding

A) Model of CARDS toxin residues 3–230 (light blue, see Experimental Procedures) superimposed on the structure of the PT-S1 subunit residues 2–201 [orange, pdb code 1bcp (Hazes et al., 1996)]. Residues of the R---STS---E signature motif found in bacterial ADP-ribosylating toxins are shown as green sticks. Conserved residues in the active site that participate in NAD+ binding and/or catalysis are shown as cyan sticks. Nitrogen atoms are color coded as blue and oxygen as red. B) Model of CARDS toxin residues 1–230 (light blue) superimposed on the structure of the CT ADPRT domain in complex with NAD$^+$ [pink, pdb code 2a5f (O'Neal et al., 2005)]. Color coding of the side chains of the signature sequence and accessory residues is the same as in the previous panel. The catalytic glutamic acid in CT was converted to an aspartic acid in this structure to prevent auto-hydrolysis of the NAD$^+$-co-factor (O'Neal et al., 2005). C) Structure of the CT ADPRT domain in complex with NAD$^+$. Orientation and color coding are the same as in the previous panels. Hydrogen bonds are shown as gray dashes and NAD$^+$ as yellow. D9 and R11 of CT form an ion-paired salt link that in turn positions the guanidinium moiety of R11 to engage in π-stacking interactions with the aromatic ring of NAD$^+$. D9 simultaneously accepts an H-bond from the epsilon nitrogen of R7 permitting the two guanidinium nitrogen atoms to donate

hydrogen bonds to each of the phosphate moieties of the co-factor. An imidazole nitrogen of H44 donates a hydrogen bond to the side chain oxygen of D112 positioning it for catalysis. D) Superposition of CARDS toxin molecular model with CT structure shown in panel C. The interactions between CARDS toxin and NAD^+ appear analogous to those of CT (and, by extension, PT). These results are consistent with the notion that CARDS toxin is a member of the CT group of bacterial ADP-ribosylating toxins.

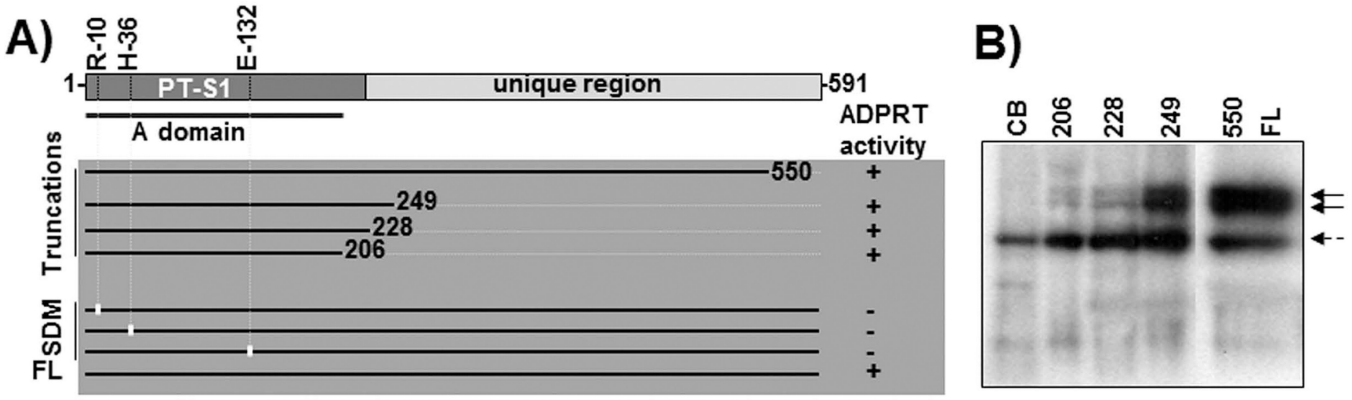

Fig. 2. N-terminal region of CARDS toxin houses ADPRT activity

A) Schematic representation of the ART activity of CARDS toxin and its derivatives. As indicated in Experimental Procedures, FL CARDS toxin, its N-terminal derivatives (truncations) and APDRT-conserved amino acid site-directed mutagenized (SDM) proteins ($Arg^{10\rightarrow Ala}$, $His^{36\rightarrow Ala}$ and $Glu^{132\rightarrow Ala}$) were analyzed for ADPRT activity, and the results are depicted. PT-S1 indicates pertussis toxin S1 catalytic subunit; FL indicates full length CARDS toxin; B) Comparison of ADP-ribosylating activity of FL and different carboxy region-deleted derivatives of CARDS toxin. Purified FL CARDS toxin and its carboxy region-truncated derivatives were individually incubated with HeLa cell lysate in the presence of ^{32}P NAD as indicated in Experimental Procedures, and the radiolabeled ADP-ribosylated proteins were detected. Each number indicates the truncated proteins depicted in Fig. 2A; CB represents carrier buffer. The two solid black arrows (~50 kDa) indicate the target ADP-ribosylated proteins of CARDS toxin, and the dotted arrow indicates the inherent ADP-ribosylated protein of mammalian cells.

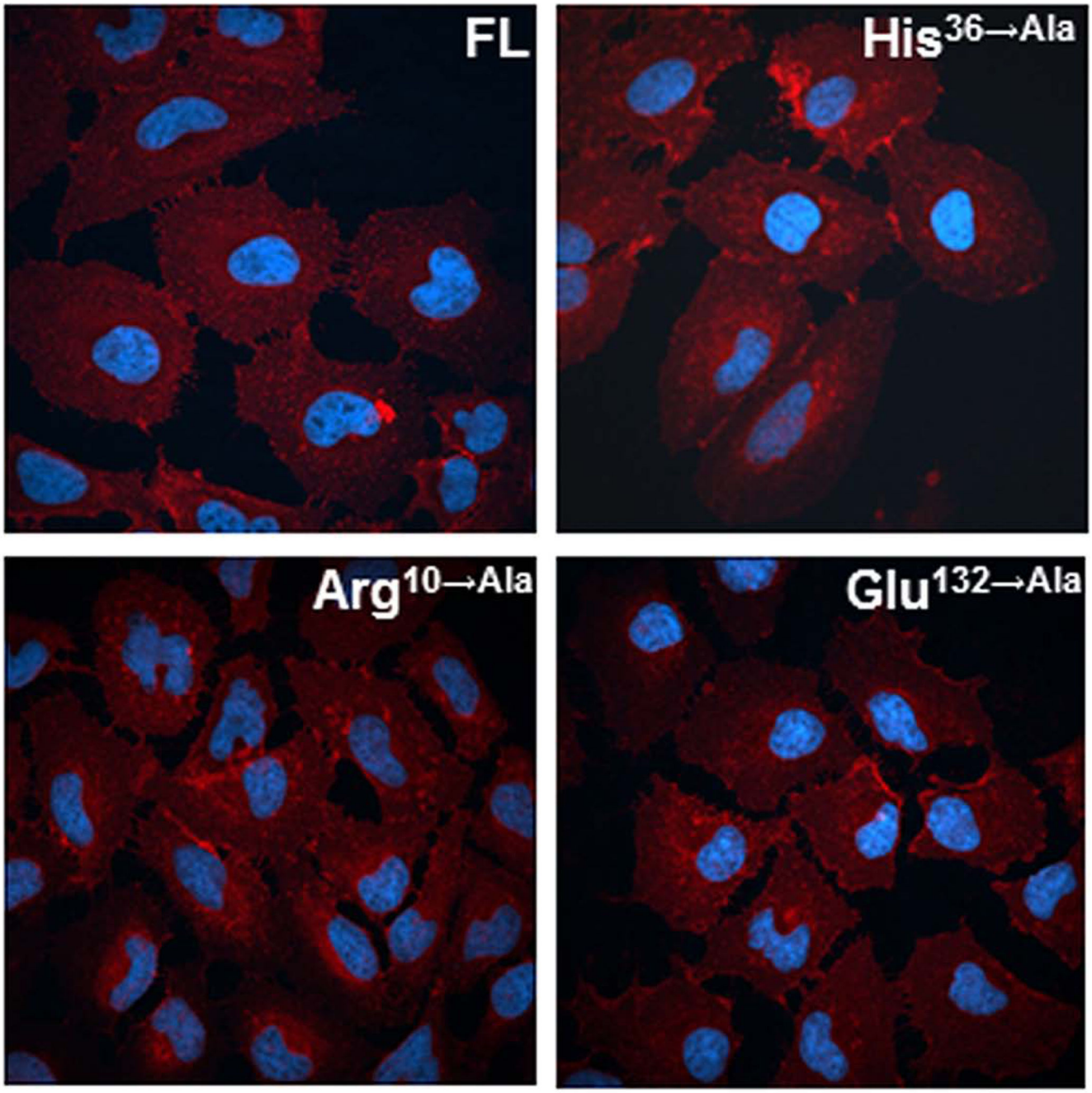

Fig. 3. Binding and internalization of CARDS toxin ADPRT mutants

HeLa cell monolayers were treated with 10 μg (≈140 pmol) of FL CARDS toxin or ADPRT mutants ($Arg^{10\rightarrow Ala}$, $His^{36\rightarrow Ala}$ and $Glu^{132\rightarrow Ala}$) at 37°C for 1h. Cells were fixed, permeabilized with 0.1% Triton X-100 and incubated with anti-CARDS toxin rabbit primary antibodies. Subsequently, cells were treated with AlexaFluor-633 conjugated goat (polyclonal) anti-rabbit secondary antibodies to detect the cellular binding and trafficking of CARDS toxin by confocal laser scanning microscopy. Cell nuclei were stained with DAPI (4',6-diamidino-2-phenylindole dihydrochloride).

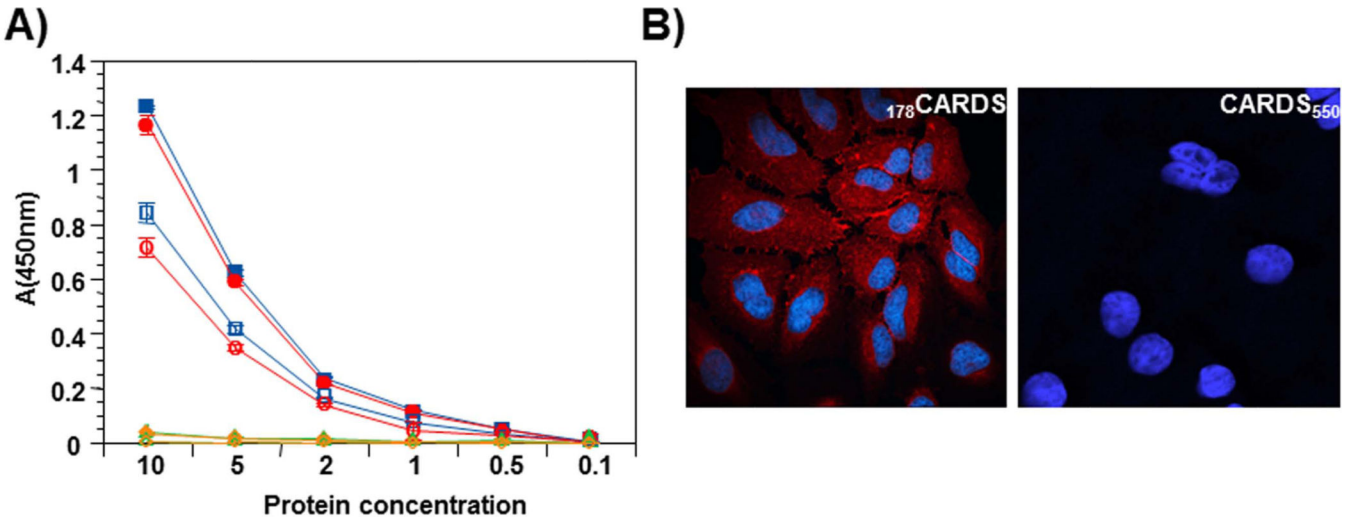

Fig. 4. Carboxy region of CARDS toxin mediates binding and internalization

A) Comparison of binding and internalization of FL, selected C-terminal truncated CARDS toxin derivatives and $_{178}$CARDS toxin. FL toxin and its derivatives were purified as indicated in Experimental Procedures and biotin labeled. *Binding*: Proteins were incubated with HeLa cells for 1 h at 4°C. Subsequently, cells were washed and bound proteins were quantified as indicated in Experimental Procedures. *Internalization*: After 1 h incubation at 4°C, bound proteins (FL, selected C-terminal truncated CARDS toxin derivatives and $_{178}$CARDS toxin) were removed by washing, and cells were shifted to 37°C for 1 h with fresh medium. Then, cells were treated with MESNA to remove surface-bound, biotin-labeled CARDS toxin and its derivatives, and internalized proteins were quantified after permeabilizing cells as indicated in Experimental Procedures. Binding and internalization results of FL and variants of CARDS toxin are shown by closed and open symbols respectively. FL - square, $_{178}$CARDS - circle, CARDS$_{249}$ - triangle and CARDS$_{550}$ - diamond. B) Endocytosis of $_{178}$CARDS toxin and CARDS$_{550}$ toxin. HeLa cells were treated with 140 pmol of $_{178}$CARDS toxin or CARDS$_{550}$ toxin for 30 min at 4°C, washed to remove unbound toxins and shifted to 37°C for 1 h. Cell preparations were fixed and permeabilized with 0.1% Triton X-100, followed by incubation with anti-CARDS toxin rabbit primary antibodies. Cells were treated with AlexaFluor-633 conjugated anti-rabbit goat (polyclonal) secondary antibodies to detect cellular binding of CARDS toxin derivatives by confocal laser scanning microscopy. Cell nuclei were stained with DAPI.

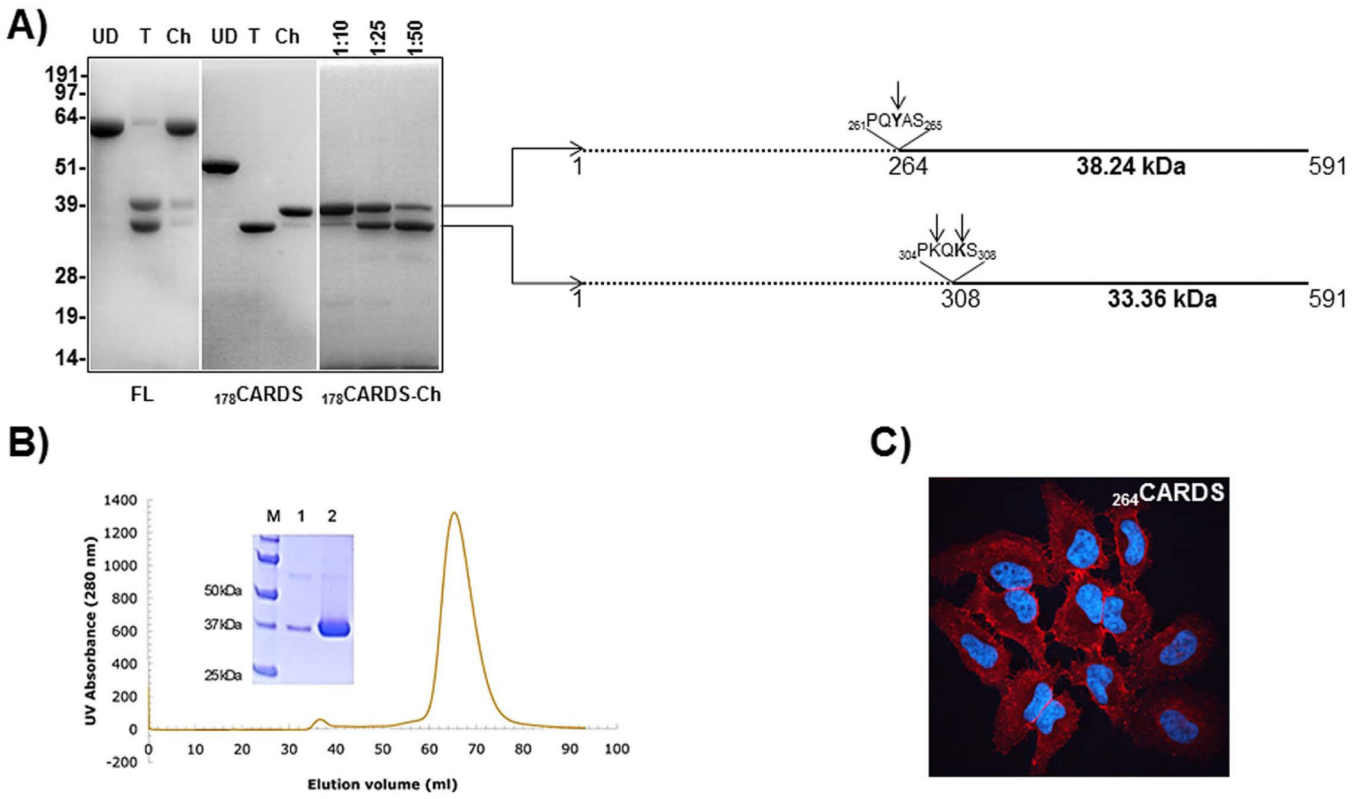

Fig. 5. Protease digestion pattern of FL and $_{178}$CARDS toxin and characterization of $_{264}$CARDS protein

A) Protease digestion patterns of FL and $_{178}$ CARDS toxin. FL and $_{178}$CARDS toxin were treated with trypsin (T) and chymotrypsin (Ch) for 30 min at room temperature. Protease digestion of the reaction mixture was arrested by adding PMSF and boiling in SDS-PAGE sample lysis buffer. Undigested (UD), T-digested and Ch-digested products of FL and $_{178}$CARDS toxin proteins were resolved on 4–12% Nu-PAGE gel and stained with Coomassie Brilliant blue. Different concentrations of Ch (ratio indicates dilution of Ch to CARDS toxin protein) used for the digestion of $_{178}$CARDS are indicated above the $_{178}$CARDS-Ch panel. N-terminal sequencing of 38 and 33 kDa proteins indicates the possible cleavage at tyrosine263 and lysine305 and 307 as represented in the schematic. B) Expression and purification of $_{264}$CARDS toxin. $_{264}$CARDS toxin was prepared as described in Experimental Procedures. Analyses of both purified peaks (small-lane 1 and large-lane 2) are shown in the Coomassie Brilliant blue stained 12% SDS-PAGE gel electrophoresis. C) Binding and internalization of $_{264}$CARDS. As indicated in Fig. 4, binding and internalization of $_{264}$CARDS were analyzed using immunofluorescence microscopy.

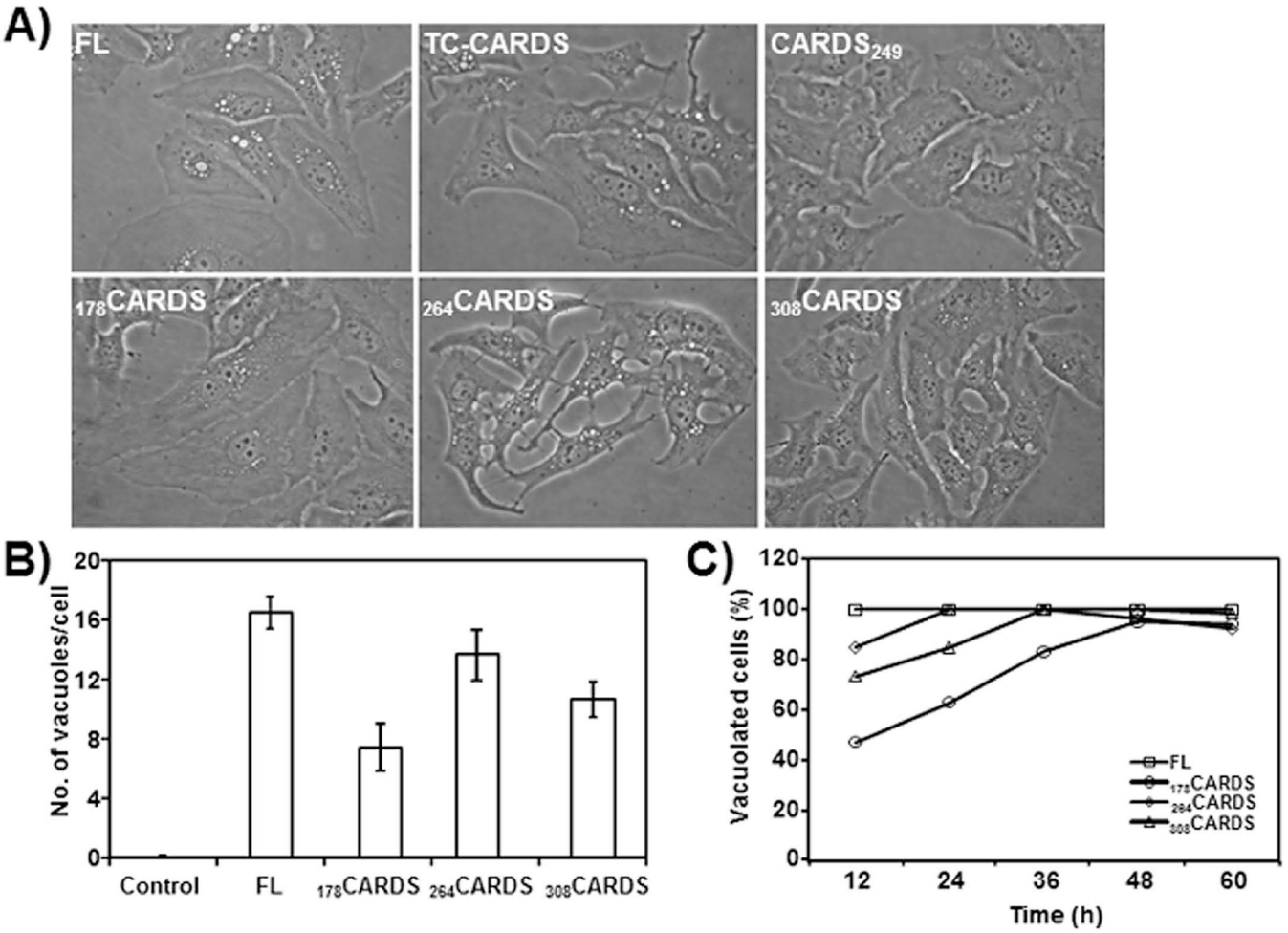

Fig. 6. Induction of vacuolization in HeLa cells by carboxy region of CARDS toxin

A) Equimolar (~140, 350 and 700 pmol) concentrations of FL, trypsin cleaved (TC), carboxy and amino terminal region truncated ($CARDS_{249}$, $_{178}CARDS$, $_{264}CARDS$ and $_{308}CARDS$) proteins were added to 60% confluent monolayer cultures of HeLa cells as indicated in Experimental Procedures and observed at 12 h to 60h. Representative images of vacuoles generated by 140 pmol concentration of proteins at 24 h are shown. Vacuoles were generated in HeLa cells by FL CARDS toxin, TC-CARDS toxin and carboxy region retaining CARDS toxin derivatives and not by $CARDS_{249}$. B) Quantification of numbers of CARDS toxin-induced vacuoles in HeLa cells incubated with FL and carboxy region variants of CARDS toxin ($_{178}CARDS$, $_{264}CARDS$ and $_{308}CARDS$) at 24 h. As indicated in section A, cells were incubated with CARDS toxin and its derivatives and vacuoles per cell were counted and compared as described in Experimental Procedures. C) Quantification of percentage of HeLa cells with CARDS-toxin induced vacuoles. As indicated in panel A, cells were incubated 12–60 h with CARDS toxin and its derivatives (140 pmol) and the number of vacuolated cells in random fields was calculated as described in Experimental Procedures.

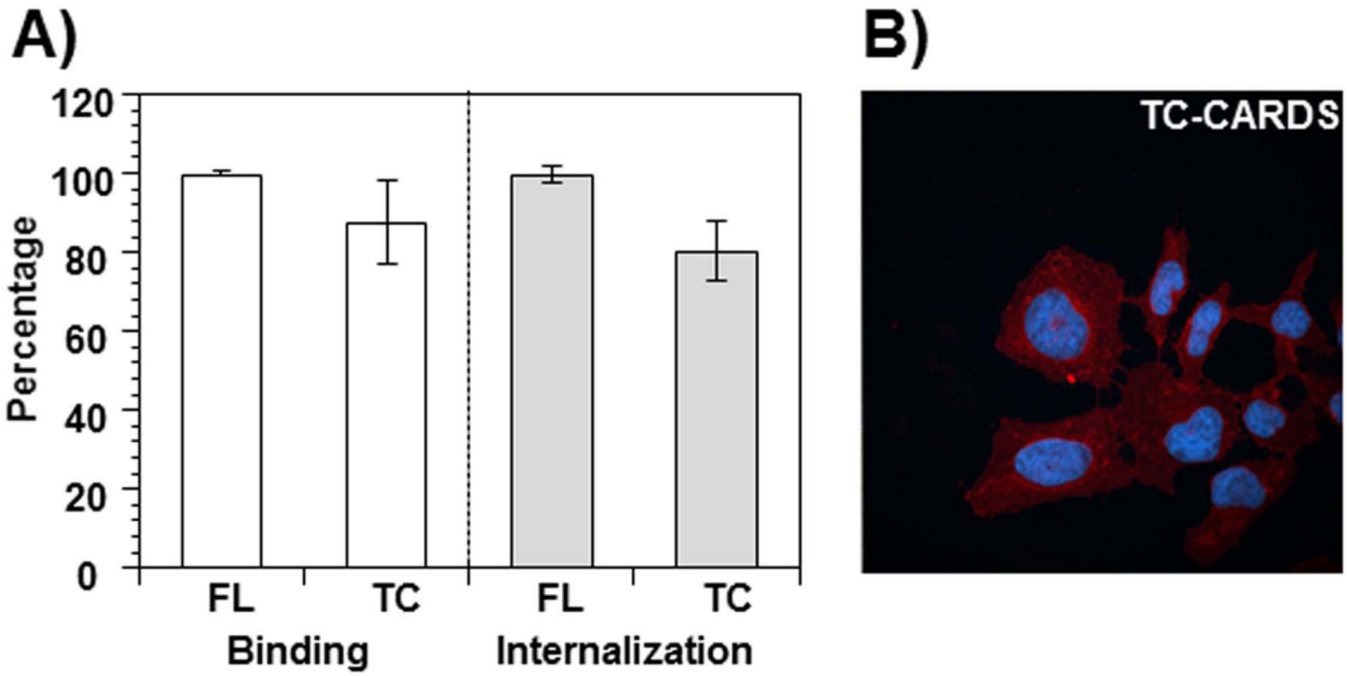

Fig. 7. Binding and internalization of trypsin-cleaved CARDS toxin

A) Comparison of binding and internalization of FL and trypsin-cleaved (TC) CARDS toxins. FL CARDS toxin was trypsin digested and purified as indicated in Experimental Procedures. FL and TC-CARDS toxins were labeled with biotin and compared for their binding and internalization properties as indicated in Fig. 6. The percentage of binding and internalization of FL and TC CARDS toxins are shown. B) Binding and internalization of TC-CARDS toxin. As indicated in Experimental Procedures, purified TC CARDS toxin was incubated with HeLa cells for 1 h at 37°C, and internalization was analyzed using immunofluorescence microscopy as indicated in Fig. 4.

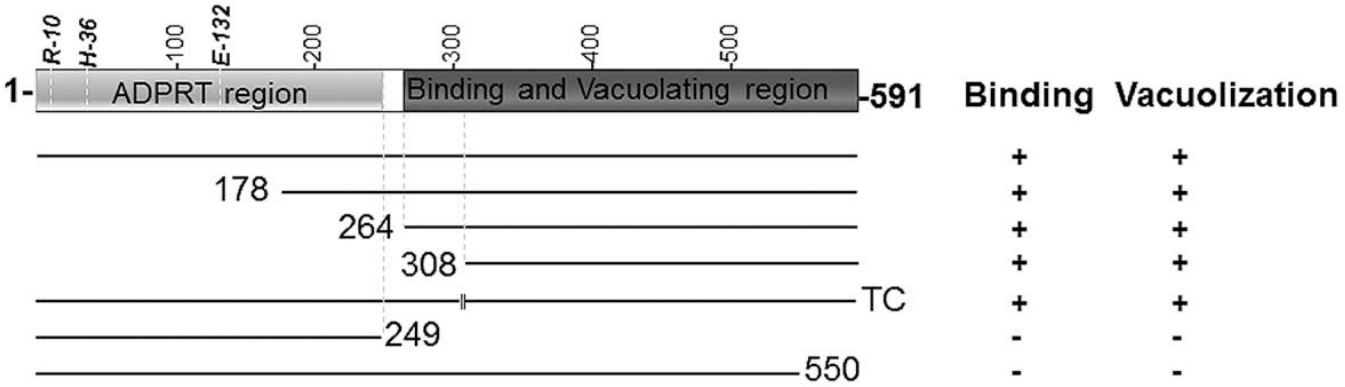

Fig. 8. Schematic diagram of CARDS toxin protein depicting the position of the ADPRT, cellular binding, and vacuolization regions

Carboxy- and N-terminal truncated CARDS toxin derivatives and their association with cellular binding, vacuolization regions are shown in dark gray. As illustrated in Fig. 2A, the identified ADPRT domain is shown in gray along with the essential amino acids.

Table 1

Top-scoring structures that can serve as templates for CARDS toxin residues 1–245 in the program MODELLER (Sanchez & Sali, 1997, Sanchez & Sali, 2000), as identified by the program HHPRED (Soding, 2005, Soding et al., 2005).

No	PDB code	Protein	Probability (percent)[a]	E-Value	P-Value	Total score[b]	Secondary structure score	No. matched columns[c]	query HMM	Template HMM
1	1bcp	Pertussis toxin (*Bordetella pertussis*)	100.0	1.3 E^{-48}	4.1E^{-53}	352.4	7.9	196	3–242	2–215 (235)
2	4k61	Typhoid toxin (*Salmonella typhi*)	100.0	1.2 E^{-46}	3.9E^{-51}	335.8	15.0	198	5–245	1–206 (224)
3	1s5d	Cholera toxin (*Vibrio cholerae*)	100.0	1.2 E^{-35}	3.7 E^{-40}	269.3	11.6	148	6–203	3–166 (240)
4	1tii	Heat labile enterotoxin (*Escherichia coli*)	100.0	1.2 E^{-35}	3.9 E^{-40}	260.8	9.9	148	6–203	1–164 (190)
5	2cb4	Mosquitocidal toxin (*Bacillus sphaericus*)	100.0	2.5 E^{-30}	8 E^{-35}	239.5	3.9	166	2–218	72–245 (291)

[a] Probability that the database match is a true positive

[b] Total score column includes the score from the secondary structure comparison.

[c] Total number of matched columns in the query-template alignment.

Table 2

Primers used for generating CARDS toxin variants

ADPRT specific primers:
R10AF- GTTAGATTTGTTTAC*GC*TGTTGATTTGAG
R10AR- CTCAAATCAACA*GC*GTAAACAAATCTAAC
H36AF- CTTTGAA*GC*CATTCTCTCCACTAATTTTGG
H36AR- CCAAAATTAGTGGAGAGAATG*GC*TTCAAAG
E132AF- GCGTATCAACGTG*C*ATGGTTTACCGAT
E132AR- ATCGGTAAACCATG*C*ACGTTGATACGC
N-terminal region primers:
187F-CCCTCATTATCAAGAGCTGTAA**A**ACCCAAGCC
187R-GGCTTGGGT**T**TACAGCTCTTGATAATGAGGG
207F-GCTACTCCTGTACATTA**A**TCAATTCCCCAAGCA
207R-TGCTTGGGGAATTGA**T**TAATGTACAGGAGTAGC
218F-CCAAGCAGCTTCCGTTGCTGATTAGTCGGAAGGTACTTCC
218R-GGAAGTACCTTCCGACTAATCAGCAACGGAAGCTGCTTGG
229F-GCTTCGCTATCGTTTTA**G**TGCCCTGATTGGAGTCC
229R-GGACTCCAATCAGGGCA**C**TAAAACGATAGCGAAGC
354F-GCGCGGTTAATTA**G**GTGAACCAAAAGTGG
354R-CCACTTTTGGTTCAC**C**TAATTAACCGCGC
392F-GGCTTGTTCTA**G**AATACCAAGAGTGGTGG
392R-CCACCACTCTTGGTATT**C**TAGAACAAGCC
448F-GTTCAGCTAGGCTA**G**TATTGGAGGGGT
448R-ACCCCTCCAATA**C**TAGCCTAGCTGAAC
508F-ACTGGTTACAGCTGGGATTA**G**GTAGAATGGC
508R-GCCATTCTAC**C**TAATCCCAGCTGTAACCAGT
526F-CGAAAACTTTAAATA**G**TACTTTTCGCGTG
526R-CACGCGAAAAGTA**C**TATTTAAAGTTTTCG
551F-CACATTCGCTGTT**TA**GCTGACAACCAGCAG
551R-CTGCTGGTTGTCAGC**TA**AACAGCGAATGTG
Specific N-terminal region amplified primers:
001F-CATATGCCAAATCCTGTTAGATTTGTTTACCGT
249R-GGATCCATCTTTT**A**CGCAATGCATTTGTCTAGCGG
307R-GGATCCCT**CT**ACTTTTGTTTGGGGTTTACTTC
C-terminal region primers:
118F-CATATGGGAATTAGAGCTTTACGCACTTC
178F-CATATGCACAACCCTCATTATCAAGAGCTG
264F-CATATGGCTAGCAGTGTAAAGGAACTGGAAG
287F-CATATGTTACAAGCAGATCCGCAAAATAAC
366F-CATATGACACCGCAAGACATTGCAATAACTC
308F-CATATGTCCAGCTTTCCCCAAACCATC

434F-CATATGCGTGCAGCTAGCACCTTCTTTGTTG

466F-CATATGAAAACACCAGATGGACAGATATTCTATG

516F-CATATGAATGAGGACAAAGACGAAAACTTTAAATG

591R-CGTTAAAGGATCCTCGCTAAAAGCGATC

Italics indicate changes from residues R or H or E to A.
Bold indicates introduced stop codon.
Underline indicates introduced NdeI and BamHI sites to clone the specific N- and C-terminal regions. F: Forward primers; R: Reverse primers